Mode-selective thermal radiation from a microsphere as a probe of optical properties of high-temperature materials

R. Morino, H. Tajima, H. Sonoda, H. Kobayashi, R. Kanamoto, H. Odashima, and M. Tachikawa
Department of Physics, Meiji University, 1-1-1 Higashimita, Tama-ku, Kawasaki, Kanagawa 214-8571, Japan
(Received 30 March 2017; published 14 June 2017)

Our spectroscopic method using laser trapping and heating has demonstrated that thermal emission from a metal oxide microsphere is enhanced at frequencies resonant with the whispering gallery modes of the spherical resonator. Only a mode series of a specific order effectively emits thermal photons, and spectral peaks shift from higher-order whispering gallery modes to fundamental whispering gallery modes as the size parameter decreases. These spectral profiles are analyzed with the Mie scattering theory and a semiclassical rate-equation model. The observed mode selectivity in thermal radiation is attributed to a matching between the rates of cavity damping and internal absorption. Excellent reproducibility of the observed spectral profiles leads to a precise determination of optical constants of extremely hot materials.

DOI: 10.1103/PhysRevA.95.063814

I. INTRODUCTION

In 1900, Max Planck established the law of blackbody radiation by introducing the idea of energy quantization of electromagnetic waves [1,2]. Planck's law of thermal radiation thus opened the door to quantum physics, and it has been utilized as a basic theory for radiation thermometry in every field of science and engineering [3].

A blackbody is an idealized object that perfectly absorbs radiations of any incidence angle, polarization, and wavelength. Planck's formula describing the spectrum of the blackbody radiation is determined only by the temperature, and is independent of any other emitter's characteristics. Thermal radiation from real objects depends on their chemical composition and surface asperities. In many cases, however, spectral emissivity of macroscopic objects is a moderate function of the wavelength, and their thermal emission spectral profile is well approximated by those of a blackbody or graybody.

If the size of a thermally excited body is comparable or smaller than thermal wavelengths, Planck's formula, derived for a macroscopic body interacting with electromagnetic waves in free-space modes, is not straightforwardly applicable. The limitations of Planck's law and size effects of thermal radiation have been the most fundamental problems in quantum optics for more than 100 years [4–7]. The issues of microthermometry are also important in rapidly developing nanotechnology and mesoscopic physics. To understand the operations of MEMS or NEMS (micro- or nanoelectromechanical systems), evaluation of each component's temperature is crucial since their motion is inevitably subject to thermal fluctuations [8]. In optomechanical systems where quantum natures of mesoscopic mechanical oscillators are explored with the aid of optical manipulations, thermal noise is a major source of quantum decoherence [9].

Nonetheless, clear experimental evidences of the size effects in thermal radiation were sparse until the last decade. Several experiments on ensembles of small particles, such as metal aerosol [10] and carbon soot [11,12], suggest that thermal radiation from those micron and submicron particles retains broadband spectral profiles well fit to Planck's formula modified with emissivity corrections. It is emphasized, however, that emission spectra normally observed in gas-flow systems or combustions are an average over samples of unidentified morphology with non-negligible size distributions. More recently, new approaches using microfabrication have revealed distinctive thermal effects of a miniature object with well-defined size, shape, and optical properties [13–17]. Experimental outcomes on the breakdown of Planck's law include thermal radiation from a thin wire with a characteristic polarization and directivity [13,14], heat transfer from a microsphere due to thermal near fields of surface phonon polaritons [15], and resonantly enhanced spectral emissivity of a thermal whisker antenna [16]. In contrast, an incandescent nanolamp made of a carbon nanotube yielded emission intensity just as predicted on the basis of Planck's law [17]. In relation to radiative energy flow from a miniature object, heat transfer across a nanometer-sized vacuum gap has also become an active research topic [15,18–20].

In our previous paper [21], we have demonstrated that the thermal radiation spectrum of a dielectric microsphere is dominated by sharp multiple peaks resonant with whispering galley modes (WGMs) of the microresonator [22,23]. Our original laser trapping technique [24] levitated a micron-sized molten drop of Al_2O_3 and enabled its emission spectroscopy as the particle gradually became smaller through evaporation. In the limited volume of the microparticle, dielectric materials interact with photons in the characteristic modes, and the rate of spontaneous emission is modified by the discrete mode density. An optically trapped microparticle is a well-defined model system to systematically explore the size effects in thermal radiation, and also provides an interesting test bench for cavity QED [25,26].

In this paper, we analyze spectral mode structures of thermal emission from a dielectric microsphere, especially focusing on the mechanism of mode selection that was not quantitatively understood in our first report [21]. By establishing a theoretical model for the radiation process, we aim to obtain a comprehensive interpretation of thermal radiation in the intermediate size parameters which bridges the gap between Planckian radiation and atomic emission. First, we take a conventional approach combining Mie scattering theory [27] and Kirchhoff's law [28]. The classical treatments precisely reproduce observed

emission spectra and their dependence on the size parameter. However, Mie formulas do not give clear insights into the mode selectivity since a contribution of each resonance mode is not explicitly expressed. We also develop a rate-equation model in which the thermal emitter is treated as an optical resonator with thermally excited two-level atoms inside. The thermal radiation spectrum is constructed from spontaneous emission power of all the resonator modes in the frequency range of interest. Mode selectivity generally observed with dielectric microparticles is straightforwardly explained by the analytic solution for the modal output power.

Another objective of this paper is to establish a methodology of precise measurements of optical constants at extremely high temperatures. Through the fittings of calculated thermal radiation spectra, one can determine the refractive index and the extinction coefficient of the medium at temperatures well over 1500 K, which are difficult to measure by conventional optical methods.

II. EXPERIMENT

In the radiation thermometry of microemitters, separating a signal of the small target from background noise is essential. It has been done in our experiment by levitating a microparticle in air with laser trapping and heating the particle directly by the laser radiation. Details of the experimental method appear in our previous papers [21,24]. In brief, the original technique of flow-assisted optical trapping uses optical gradient forces from retroreflected horizontal CO_2 laser beams. The laser trap is installed in a vacuum chamber filled with air of low pressure around 2 kPa. Convective airflow directed upward in the trap region partly cancels gravity and markedly improves stability of the optical levitation. A microparticle is produced inside the trap by laser ablation of coarse-grained powders of TiO_2, Al_2O_3, or ZrO_2. These metal oxide materials have absorption bands around 10μm associated with lattice vibrations. The particle, being trapped and heated to over 2000 K by the infrared radiation, emits thermal photons in the visible to infrared frequency range. As an example, Fig. 1 shows a charge-coupled device (CCD) image of a TiO_2 microparticle thermally emitting white light with a sample tray from which TiO_2 powders are launched into the CO_2 laser beam.

FIG. 1. Image of a TiO_2 microparticle thermally emitting white light. Seen below is a sample tray.

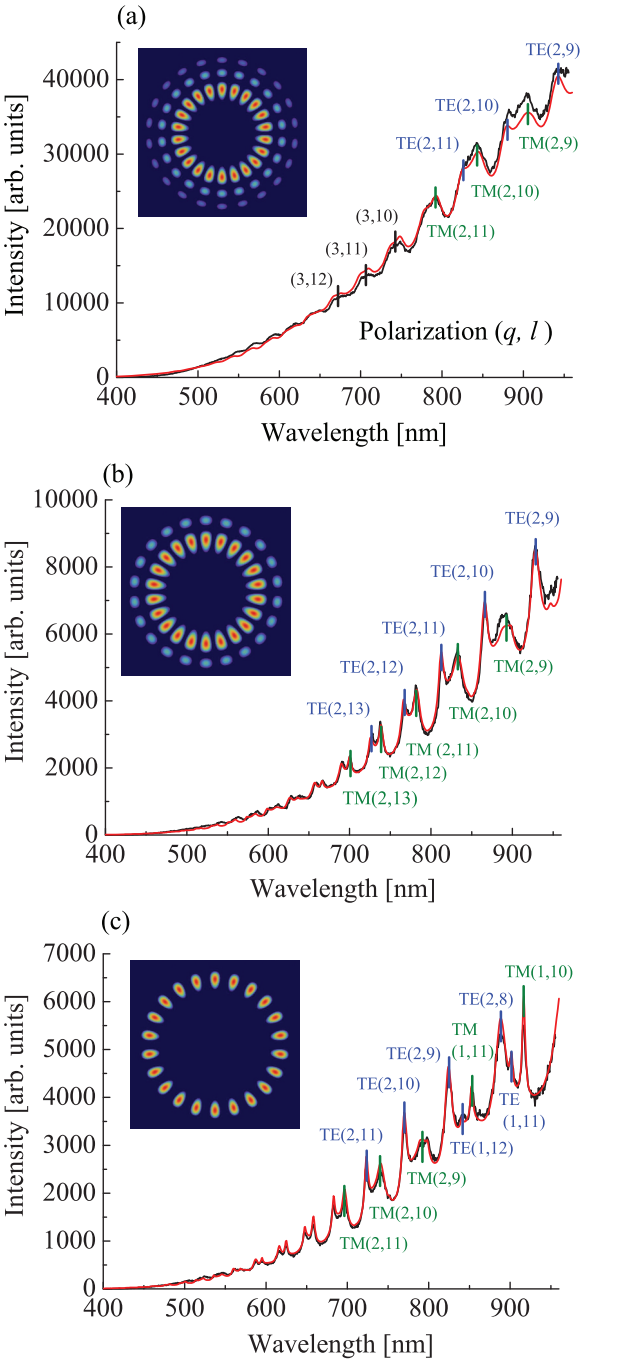

FIG. 2. Emission spectrum of a single TiO_2 particle as it shrinks due to sublimation. Observed and calculated spectra are drawn in black and red. Assignments of WGM peaks are shown with polarization and indices (q, l). Examples of WGM pattern with $(q = 3,2,1, l = m = 11)$ are inserted. Spectral profiles are best fitted with (a) $d = 2.35\,\mu$m, $T = 2010$ K, and $\kappa = 18 \times 10^{-3}$; (b) $d = 2.31\,\mu$m, $T = 1820$ K, and $\kappa = 6 \times 10^{-3}$; and (c) $d = 2.05\,\mu$m, $T = 1860$ K, and $\kappa = 5 \times 10^{-3}$.

Thermal emission spectrum of the trapped high-temperature particle drastically changes as it shrinks due to evaporation. Fig. 2 shows time evolution of the visible emission spectrum of a single TiO_2 particle. According to the analysis described below, the particle is a sphere with a

diameter d of 2.0−2.5 μm and a temperature T of 1800–2100 K. It is reasonably speculated that the TiO_2 particle once melts in the process of laser ablation to become a spherical molten droplet, and then cools down to solidify below the melting point of 2113 K. As the particle becomes smaller, a blackbodylike spectrum turns into a spectrum dominated by multiple peaks resonant with whispering gallery modes of the spherical resonator.

Characteristic modes of a dielectric spherical resonator are specified by polarization (TE or TM) and three indices l, q, m ($|m| \leqslant l$), where l is approximately the number of wavelengths in the circumference of the sphere, q is the number of field maxima in the radial direction, and $l - |m| + 1$ is the number of field maxima in the polar direction [22,23]. In a perfect sphere, modes are degenerate with respect to m. Typical whispering gallery waves, which travel around the equator of the sphere via total internal reflections, correspond to the modes with large l ($|m| \cong l$) and $q = 1$. The modes with $q > 1$ but close to unity are often called higher-order whispering gallery modes [23].

All distinctive peaks in the observed thermal radiation spectra have been assigned as indicated by mode numbers in Figs. 2(a)–2(c). In Fig. 2(a), the spectrum is modulated by broad resonances due to TE and TM modes with $q = 3$ for shorter wavelengths and those with $q = 2$ for longer wavelengths. For a smaller diameter of the same particle, the whole spectrum is dominated by narrower resonant peaks of the $q = 2$ mode series. When the particle diameter becomes as small as 2.0 μm, very sharp resonances with the most fundamental $q = 1$ modes appear in the near-infrared spectral range. As examples, mode patterns of WGM with ($q = 3,2,1$, $l = m = 11$) are depicted.

It should be noted that thermal radiation is not enhanced at all frequencies resonant with the resonator modes, but specific modes effectively emit thermal photons. As the size parameter $x \equiv \pi d/\lambda$ becomes smaller, the selected WGMs shift to lower orders, being more localized near the boundary surface. This tendency was observed also with Al_2O_3 [21] or ZrO_2 microparticles, and it is a general effect in thermal radiation from dielectric thermal emitters.

III. MIE SCATTERING THEORY

The spectral emissivity of a particle is defined as the ratio of the power thermally emitted by the particle in unit frequency interval $p(\nu)$ to that of an imaginary blackbody of the same morphology $p_{\mathrm{BB}}(\nu)$, and for a sphere of diameter d, it is expressed as [29]

$$e = \frac{p(\nu)}{p_{\mathrm{BB}}(\nu)} = \frac{p(\nu)}{\pi^2 d^2 I_{\mathrm{BB}}(\nu)}. \tag{1}$$

Here $I_{\mathrm{BB}}(\nu) = \frac{2h\nu^3}{c^2}\frac{1}{\exp(h\nu/k_BT)-1}$ is Planck's formula for the spectral radiance. According to Kirchhoff's law of thermal radiation [28] that describes detailed balance at every spectral component in thermal equilibrium, the spectral emissivity is equal to the absorption efficiency a for incoming radiation. If we assume that a hot particle of temperature T placed in a cold space emits thermal radiation in the same manner as in thermal equilibrium with environmental electromagnetic fields, the spectrum of thermal radiation from the particle is given by

$$p(\nu) = \pi^2 d^2 e I_{\mathrm{BB}}(\nu) = a\frac{2\pi^2 d^2 h\nu^3}{c^2}\frac{1}{\exp(h\nu/k_BT) - 1}. \tag{2}$$

The absorption efficiency is calculable from the sphere's Mie scattering coefficients $a_l(x)$ and $b_l(x)$ as follows:

$$a = \frac{2}{x^2}\sum_{l=1}^{\infty}(2l+1)[\mathrm{Re}(a_l + b_l) - (|a_l|^2 + |b_l|^2)], \tag{3}$$

$$a_l(x) = \frac{N^2 j_l(Nx)[x j_l(x)]' - j_l(x)[Nx j_l(Nx)]'}{N^2 j_l(Nx)\left[x h_l^{(1)}(x)\right]' - h_l^{(1)}(x)[Nx j_l(Nx)]'}, \tag{4}$$

$$b_l(x) = \frac{j_l(Nx)[x j_l(x)]' - j_l(x)[Nx j_l(Nx)]'}{j_l(Nx)\left[x h_l^{(1)}(x)\right]' - h_l^{(1)}(x)[Nx j_l(Nx)]'}, \tag{5}$$

where $N = n + i\kappa$ is the complex refractive index of the particle, $j_l(x)$ is the first kind of spherical Bessel function of the order l, and $h_l^{(1)}(x)$ is the first kind of spherical Hankel function of the order l. We have assumed that the particle is nonmagnetic and suspended in vacuum. Derivation of these formulas appears in the literature [27,29]. In brief, let a monochromatic plane wave be incident upon a sphere. The incident electromagnetic fields, scattered fields, and internal fields may be expanded in an infinite series of vector spherical harmonics. The coefficients $a_l(x)$ and $b_l(x)$ describe the amplitude of the spherical harmonics of the order l in the scattered fields: $a_l(x)$ corresponds to the TM wave and $b_l(x)$ to the TE wave. Boundary conditions on the sphere surface yield explicit solutions (4) and (5). The absorption efficiency is obtained from extracting the scattering efficiency from the extinction efficiency of the incident wave.

Figures 2(a)–2(c) show thermal radiation spectra calculated from Eqs. (2) and (3) with fitting parameters d, T, n, and κ. Resonances of the spherical resonator occur at size parameters that make the denominators of $a_l(x)$ or $b_l(x)$ close to zero. For a given order of l, there are an infinite number of resonance frequencies, and they are identified by a newly introduced index q [23]. Mode numbers (q,l) and polarization (TE or TM) assigned to the spectral peaks are shown in the figure. Several features in the spectral profiles are critically influenced by a specific parameter. The optical constants n and κ are uniquely determined from relative position and shape of the spectral resonances. The extinction coefficient κ is assumed to be independent of wavelength in the observation range. This approximation is reasonably verified for these dielectrics whose interband and phonon transitions are in the UV and mid-IR ranges, respectively. For better matching, however, the refractive index n is assumed to slightly depend on wavelength. A detailed procedure for determining those optical parameters is described below. Once the refractive index is fixed, the particle diameter is determined with equal precision from the free spectral range of the WGMs. As can be seen in Eq. (2), the choice of temperature does not affect the resonance structures but varies the gradient of the spectral base.

The observed spectral profiles are reproduced by theoretical curves with excellent fidelity, suggesting that this Mie-theory-

based treatment correctly describes essential processes of the mode-selective thermal radiation. However, it is not straightforward from Eq. (3) which modes are most enhanced and how the dominant modes shift with the size parameter. In the next section, we clarify the mechanism of the mode selectivity by calculating thermal energy distributed to a single mode of the microresonator with rate equations.

IV. RATE-EQUATION MODEL

Our rate-equation model treats the micron-sized dielectric particle as an optical cavity containing two-level atoms. The two-level atoms interact with electromagnetic fields inside the resonator to emit or absorb photons in the cavity modes. In this simplified model, the energy exchange between matter and electromagnetic fields is described by rate equations for photon numbers and atomic populations without taking their spatial distributions into account.

Following the theory of microcavity lasers [30], creation and annihilation of photons in a specific cavity mode are expressed as

$$\frac{ds}{dt} = A(s+1)N_2 - AsN_1 - \gamma s, \tag{6}$$

where s denotes the number of photons in the mode of interest, N_1 and N_2 are the numbers of lower- and upper-state atoms inside the mode volume, and γ is the rate of cavity damping due to the out-coupling of radiation. The rate of spontaneous emission into this mode A is calculated from Fermi's golden rule, according to which the transition rate of an excited atom is given by

$$S_{\text{emis}} = \frac{2\pi^2\mu^2}{\varepsilon_0 h^2 V}\int_0^\infty h\nu(s+1)g_c(\nu)g_a(\nu)d\nu. \tag{7}$$

Here μ is the atomic transition dipole moment and V is the mode volume. $g_c(\nu)$ and $g_a(\nu)$ represent normalized spectral profiles of the electromagnetic field and the atomic transition, respectively. The former is sharply peaked around the resonance frequency of the cavity ν_c, and the latter is a slowly varying function of frequency since these metal oxide dielectrics have broadband absorption. Then, the transition rate is reasonably approximated as

$$S_{\text{emis}} = \frac{2\pi^2\mu^2}{\varepsilon_0 h^2 V} h\nu_c g_a(\nu_c)(s+1) \equiv A(s+1). \tag{8}$$

The emission rate A is related to the power absorption coefficient α by $\alpha = \frac{A(N_1-N_2)}{c'}$, where c' is the speed of light in the medium.

If the atomic populations obey a Boltzmann distribution of temperature T, the number of photons in the steady state is written as

$$\bar{s} = \frac{AN_2}{A(N_1-N_2)+\gamma} = \frac{c'\alpha(\nu_c)}{c'\alpha(\nu_c)+\gamma}\frac{1}{\exp(h\nu_c/k_BT)-1}. \tag{9}$$

The radiation power coupled out of the single mode is equal to $\gamma\, h\nu_c\, \bar{s}$. The whole spectrum of thermal radiation power emitted from the microresonator is obtained by summing

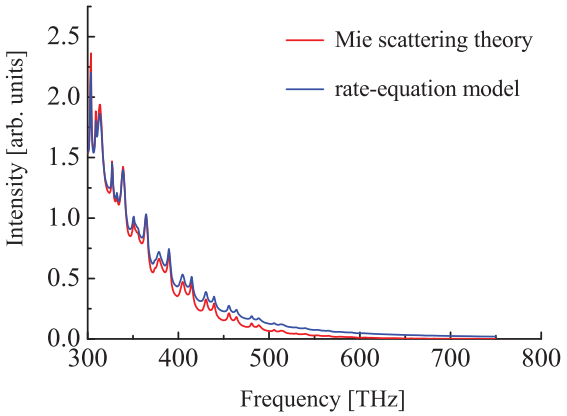

FIG. 3. Thermal emission spectrum calculated from the rate-equation model (blue curve) and that from the Mie scattering theory (red curve) for the same parameters, $d = 2.23\ \mu$m, $T = 1900$ K, $n = 2.05$, and $\kappa = 5 \times 10^{-3}$.

contributions from all the modes in the observation bandwidth,

$$p(\nu) = \sum_i \frac{c'\alpha(\nu_{ci})\gamma_i}{c'\alpha(\nu_{ci})+\gamma_i}\frac{h\nu_{ci}}{\exp(h\nu_{ci}/k_BT)-1}m_i(\nu). \tag{10}$$

Here $\nu_{ci}, \gamma_i, m_i(\nu)$, respectively, represent the center frequency, the damping rate, and the spectral density of the ith cavity mode. The mode density is reasonably approximated to the Lorentzian function:

$$m_i(\nu) = \frac{1}{\pi}\frac{\Delta\nu_i}{(\nu-\nu_{ci})^2+\Delta\nu_i^2}. \tag{11}$$

The center frequency and the half width of the spectrum $\Delta\nu_i$ are real and imaginary parts of the natural frequency derived from the boundary conditions for a dielectric sphere. They depend on the size of the sphere, the refractive index n, and the extinction coefficient κ of the dielectric medium. The extinction coefficient is related to the power absorption coefficient by $\alpha = 4\pi\kappa/\lambda$. The imaginary part of the natural frequency corresponds to the rate of electric-field damping due to internal absorption and out-coupling, and is written as

$$\Delta\nu_i = \frac{c'\alpha(\nu_{ci})+\gamma_i}{4\pi}. \tag{12}$$

The cavity damping rate γ_i is obtained from the imaginary part of the natural frequency when there is no absorption.

Figure 3 compares two thermal emission spectra calculated according to Eqs. (10) and (2) for the same parameters $d = 2.23\,\mu$m, $T = 1900$ K, $n = 2.05$, and $\kappa = 5 \times 10^{-3}$. Their similarity confirms consistency between the semiclassical rate-equation analysis and the classical analysis based on Mie theory and Kirchhoff's law. Kirchhoff's law of thermal radiation is a sufficient condition to maintain detailed balance in thermal equilibrium. Whether this law is applicable to a nonequilibrium situation such as a thermal emitter placed in a cold environment has been a subject of controversy [31]. The present rate-equation model, which describes thermal emission into a cold space, verifies the use of Kirchhoff's law in the nonequilibrium case. The model can be extended to the case where the emitting body and its environment are characterized by the same temperature. Simple calculation shows that the

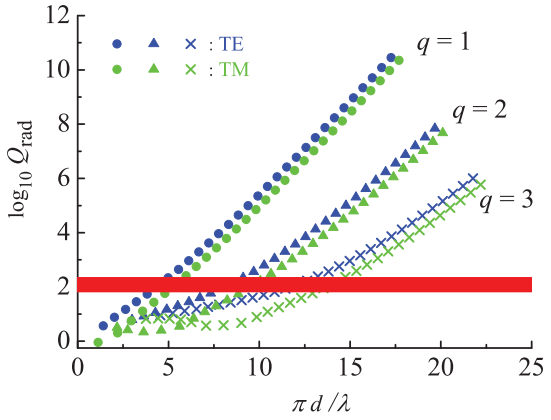

FIG. 4. $Q_{\rm rad}$ of WGMs with $q = 1 - 3$ as a function of the size parameter. The red band represents an absorptive Q factor.

power spectrum given by Eq. (10) is modified into the product of Planck's formula and the sum of the absorption efficiency of each mode in thermal equilibrium.

V. DISCUSSION

Selective enhancement of the whispering gallery modes is well understood from Eq. (10). The spectral peak power of the ith mode is written as

$$p_{\max,i} = \frac{4c'\alpha(\nu_{ci})\gamma_i}{[c'\alpha(\nu_{ci}) + \gamma_i]^2} \frac{h\nu_{ci}}{\exp(h\nu_{ci}/k_B T) - 1}. \quad (13)$$

The leading factor, which takes a maximum when $c'\alpha(\nu_{ci}) = \gamma_i$, determines the most dominant resonator modes; a mode whose out-coupling radiative loss matches the internal absorption most efficiently emits photons to outer space. This is analogous to the impedance matching in an electric circuit. The energy extracted from a battery is maximal when the external resistance is equal to the internal resistance of the battery.

From Eq. (12), the quality factor of a resonator mode Q_i is expressed with two partial quality factors, $Q_{\rm rad}$ and $Q_{\rm abs}$, relating to radiative decay and internal absorption,

$$\frac{1}{Q_i} = \frac{2\Delta\nu_i}{\nu_{ci}} = \frac{\gamma_i}{\omega_{ci}} + \frac{2\kappa}{n} = \frac{1}{Q_{\rm rad}} + \frac{1}{Q_{\rm abs}}. \quad (14)$$

Figure 4 plots $Q_{\rm rad} = \frac{\omega_{ci}}{\gamma_i}$ for spherical resonator modes with $q = 1 - 3$ as a function of the size parameter. If the size parameter is well over 10, the radiative quality factor of both TE and TM modes monotonically increases with the size parameter, and higher-order WGMs have lower Q values. Impedance matching occurs where $Q_{\rm rad}$ crosses the absorptive quality factor $Q_{\rm abs}$ which is constant with respect to the size parameter in the present case of TiO_2. As the particle becomes smaller, most enhanced mode series shift to lower q. Or for a fixed particle size, low-q modes better satisfy the matching condition at longer wavelengths and high-q modes at shorter wavelengths.

Temperature dependence of the extinction coefficient is also responsible for the selection of the enhanced mode series, especially for a transition from Figs. 2(a) to 2(b). During the interval, the trapped particle cools down from 2010 to 1820 K, and the best fit value of κ decreases threefold, suggesting that κ is a rapidly increasing function of T. In Fig. 4, the red band shows the extent of the absorptive Q factor. As the particle cools down, the absorptive Q factor increases and selected modes shift to lower-q series with higher Q factors.

The rate-equation model intrinsically involves macroscopic and microscopic limits in the emitter size. In the limit of $Q_{\rm rad} \gg Q_{\rm abs}$ or $c'\alpha(\nu_{ci}) \gg \gamma_i$ corresponding to a very large object with extremely slow cavity damping, the photon number in each mode reaches its thermal equilibrium value and the emission spectrum loses characteristics of the material. If the out-coupling efficiency is mode independent, just as a hole on a cavity wall small enough but much larger than thermal wavelengths, the spectrum described by Eq. (10) approaches Planck's formula of blackbody radiation. In the opposite case of a very small object with fast cavity damping, $Q_{\rm rad} \ll Q_{\rm abs}$ or $c'\alpha(\nu_{ci}) \ll \gamma_i$, the emission spectrum becomes proportional to the absorption coefficient of the medium. Further taking a limit to a point emitter conflicts with several assumptions made in the analysis. Yet asymptotic behavior is qualitatively described along the present model; the number of photons emitted per unit time from a single mode is equal to AN_2, implying that photons, once spontaneously emitted, leave the cavity before being absorbed and reemitted by atoms, and their spectrum directly determines that of the thermal radiation of the microcavity. In this limit, cavity mode density severely broadens and loses resonance structures, so the frequency of emitted photons is pulled into the atomic resonance, as in the case of spontaneous emission from atoms in free space.

Finally, the validity of measuring the optical constants from thermal radiation spectra is considered. Since the Mie-theory-based calculation reproduces observed spectra with excellent fidelity, we use Eq. (2) as a fitting function. The refractive index can be determined with high precision by use of sensitive dependence of the WGM frequencies on this parameter. The phase shift upon internal reflections is different for TE and TM modes, and it causes a separation of their resonance frequencies. The ratio of the separation to a free spectral range depends only on the refractive index [23] and is a key feature in its determination. If we neglect dispersion and employ a constant value for n, a systematic discrepancy appears in the position of WGMs between the observed and calculated spectra. To compensate for this discrepancy, wavelength-dependent refractive index is introduced into the Mie coefficients. Figure 5(a) shows the value of n obtained from the mode spacing of each WGM as a function of wavelength. The relative precision of each refractive index data point is estimated to be within a few percent, limited by resolutions of the WGM peaks. The fitted curve, $n = 2.434(77) - 0.70(19)\lambda\ (\mu\text{m}) + 0.34(12)\lambda\ (\mu\text{m})^2$, reasonably exhibits normal dispersion. It is actually used in the calculation of spectral profiles of Figs. 2(a)–2(c). The ordinary refractive index of TiO_2 (rutile) bulk crystals at room temperature is 2.7 at 500 nm and 2.5 at 900 nm [32]. The fitted curve gives values systematically smaller than the crystal data. There are no data of the optical constants of TiO_2 measured at temperature as high as 2000 K. The thermal coefficient of the refractive index of TiO_2 is negative but it is as small as 10^{-5}/K [33]. It is not sensible to attribute the discrepancy only to temperature differences. At high temperatures, crystallinity and even stoichiometry could be different from those at room

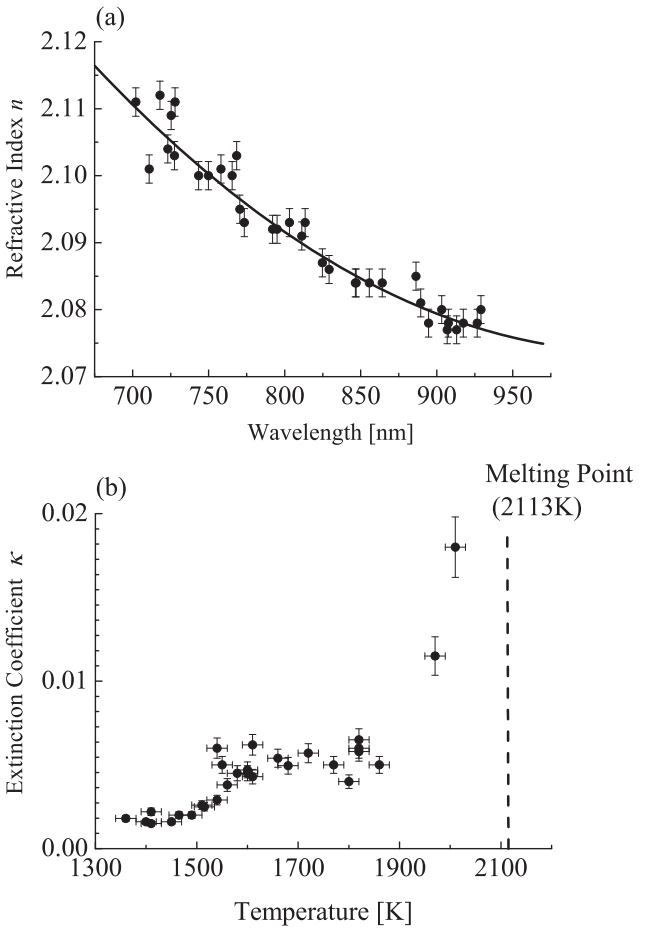

FIG. 5. (a) Refractive index of TiO_2 determined by the fittings of theoretical curves to the observed spectra. The solid curve represents a best-fit quadratic function. (b) Extinction coefficient of TiO_2 determined by the spectral fittings. Data of four different particles were collected. Error bars represent uncertainties in the spectral fitting.

temperature. The refractive indices of TiO_2 thin films range from 1.8 to 2.7 over the visible region (500–900 nm) depending on the process in deposition or annealing [34,35].

While the refractive index determines the resonance frequencies, the extinction coefficient affects the width of the resonances. Figure 5(b) shows the values of κ vs T, obtained from the spectral fitting of several TiO_2 particles. The extinction coefficient thus determined in the visible region ranges from 10^{-3} to 10^{-2} and rapidly increases with temperature. Extinction coefficients of TiO_2 thin films measured at room temperature are of the order of $10^{-4} - 10^{-1}$ [34,35]. Again, no data to be compared are available around 2000 K, but it has been reported that absorbance of Al_2O_3 for visible and short-wave IR radiation drastically increases with temperature around the melting point [36,37]. Transparent dielectric materials like TiO_2 may exhibit the same tendency.

VI. CONCLUSION

We have observed selective enhancement of a specific WGM series in thermal radiation spectra of a dielectric microsphere. Dominant emission shifts from higher-order WGMs to fundamental WGMs as the size parameter decreases. Our rate-equation model has provided a clear understanding that mode selection is caused by the matching between the internal absorptive loss and the out-coupling cavity damping of thermally emitted photons. An analytic expression for the spectral profile gives insight into a transition from macroscopic blackbody radiation to microscopic atomic emission. The present semiclassical approach is generally applicable to the analysis of thermal emission in a closed space, such as sonoluminescence from microcavitations [38].

From one-to-one correspondence of the observed spectral profiles and those reproduced from the Mie scattering coefficients, optical constants of high-temperature dielectric materials were determined. Resonance structure of a microsphere is a sensitive probe for those optical properties. The present analysis will benefit investigations of high-temperature phenomena such as liquid-solid phase transitions and transitions between crystal structures. To confirm its reliability, however, identification of the chemical composition and crystallinity of the microparticles is crucial.

A high-temperature microsphere is a useful test bench for light-matter interactions in a limited volume. Future prospects on thermal radiation from optically levitated dielectric particles include the cavity QED effect of dopant atoms coupled with WGMs [25,26], surface phonon polariton resonance [39], and surface plasmon resonance of metal nanoparticles [40] embedded in the dielectric medium.

ACKNOWLEDGMENTS

The authors gratefully acknowledge N. Kase, K. Nagase, T. Ehara, S. Sato, and K. Inoue for their assistance in experiments and numerical analysis. This work was supported by JSPS Grant-in-Aid for Scientific Research (Grant No. 26400420).

[1] M. Planck, Verhandl. Dtsch. Phys. Ges. **2**, 202 (1900).
[2] M. Planck, Verhandl. Dtsch. Phys. Ges. **2**, 237 (1900).
[3] M. Q. Brewster, *Thermal Radiative Transfer and Properties* (Wiley, New York, 1992).
[4] S. C. Ching, H. M. Lai, and K. Young, J. Opt. Soc. Am. B **4**, 1995 (1987).
[5] S. Lange and G. Schweiger, J. Opt. Soc. Am. B **11**, 2444 (1994).
[6] K. Hansen and E. E. B. Campbell, Phys. Rev. E **58**, 5477 (1998).
[7] A. M. Garcia-Garcia, Phys. Rev. A **78**, 023806 (2008).
[8] K. L. Ekinci and M. L. Roukes, Rev. Sci. Instrum. **76**, 061101 (2005).
[9] M. A. Page, Ch. Zhao, D. G. Blair, L. Ju, Y. Ma, H.-W. Pan, Sh. Chao, V. P. Mitrofanov, and H. Sadeghian, J. Phys. D: Appl. Phys. **49**, 455104 (2016).
[10] Y. Murakami, T. Sugatani, and Y. Nosaka, J. Phys. Chem. A **109**, 8994 (2005).
[11] J. D. Eversole, Appl. Opt. **23**, 3439 (1984).
[12] E. A. Rohlfing, J. Chem. Phys. **89**, 6103 (1988).

[13] C. Wuttke and A. Rauschenbeutel, Phys. Rev. Lett. **111**, 024301 (2013).
[14] V. A. Golyk, M. Kruger, and M. Kardar, Phys. Rev. E **85**, 046603 (2012).
[15] S. Shen, A. Narayanaswamy, and G. Chen, Nano Lett. **9**, 2909 (2009).
[16] J. A. Schuller, T. Taubner, and M. L. Brongersma, Nat. Photonics **3**, 658 (2009).
[17] Y. Fan, S. B. Singer, R. Bergstrom, and B. C. Regan, Phys. Rev. Lett. **102**, 187402 (2009).
[18] K. Kim, B. Song, V. Fernandez-Hurtado, W. Lee, W. Jeong, L. Cui, D. Thompson, J. Feist, M. T. Homer Reid, F. J. Garcia-Vidal, J. C. Cuevas, E. Meyhofer, and P. Reddy, Nature **528**, 387 (2015).
[19] K. Kloppstech, N. Konne, S.-A. Biehs, A. W. Rodriguez, L. Worbes, D. Hellmann, and A. Kittel, Nat. Commun. **8**, 14475 (2017).
[20] S. Edalatpour and M. Francoeur, Phys. Rev. B **94**, 045406 (2016).
[21] H. Odashima, M. Tachikawa, and K. Takehiro, Phys. Rev. A **80**, 041806(R) (2009).
[22] J. A. Stratton, *Electromagnetic Theory* (McGraw-Hill, New York, 1941).
[23] A. N. Oraevsky, Quantum Electron. **32**, 377 (2002).
[24] T. Ochiai, M. Numoto, M. Tachikawa, and H. Odashima, Jpn. J. Appl. Phys. **46**, L957 (2007).
[25] E. M. Purcell, Phys. Rev. **69**, 681 (1946).
[26] D. Kleppner, Phys. Rev. Lett. **47**, 233 (1981).
[27] G. Mie, Ann. Phys. **25**, 377 (1908).
[28] G. Kirchhoff, Ann. Phys. Chem. **109**, 275 (1860).
[29] C. F. Bohren and D. R. Huffman, *Absorption and Scattering of Light by Small Particles* (John Wiley and Sons, New York, 1998).
[30] H. Yokoyama and S. D. Brorson, J. Appl. Phys. **66**, 4801 (1989).
[31] H. P. Baltes, Prog. Opt. **13**, 1 (1976).
[32] T. Toyoda, J. Phys. D **18**, L129 (1985).
[33] T. Toyoda and M. Yabe, J. Phys. D **16**, L251 (1983).
[34] D.-J. Won, C.-H. Wang, H.-K. Jang, and D.-J. Choi, Appl. Phys. A **73**, 595 (2001).
[35] B. S. Richards, Sol. Energy Mater. Solar Cells **79**, 369 (2003).
[36] E. J. Mularz and M. C. Yuen, J. Quantum Spectrosc. Radiat. Transfer **12**, 1553 (1972).
[37] V. Sarou-Kanian, J. C. Rifflet, and F. Millot, Int. J. Thermophys. **26**, 1263 (2005).
[38] P.-K. Choi, S. Abe, and Y. Hayashi, J. Phys. Chem. B **112**, 918 (2008).
[39] J. Pastrnak and K. Vedam, Phys. Status Solidi **3**, 647 (1970).
[40] C. Noguez, J. Phys. Chem. C **111**, 3806 (2007).